Towards reliability-based geometry optimization of a point-absorber with PTO reliability objectives

Caitlyn E. Clark, Anna Garcia-Teruel, Bryony DuPont, and David Forehand

***Abstract*—In this study, we seek to understand the relationship between wave energy converter (WEC) hull geometries and power take-off (PTO) reliability. To do this, we calculate the damage equivalent loads (DELs) for a PTO given three hull shapes (a cylinder, a sphere, and a barge), two sets of metocean conditions (from the center of the North Sea and off the west coast of Norway), and two float motions (heave and surge). Results indicate that hull geometry has a primary influence on DELs experienced by the PTO, and also that certain geometries result in larger variations in DELs based on whether the device is moving in heave or surge motion. These findings underline the importance of considering WEC hull geometry in early design processes to optimize cost, power production, and reliability. More importantly, this research emphasizes the need to consider the relationship between the WEC geometry and the PTO reliability early in the design process. By considering this relationship, more optimal WECs can be designed for power production and system reliability. The methods tested in this study will enable the future reliability-based geometry optimization of WEC hulls to maximize reliability and power production.**

***Index Terms*—reliability-based design, PTO, wave energy, point absorber**

I. Introduction

As the wave energy industry progresses towards commercialization, research and development efforts to characterize and improve reliability of wave energy converters (WECs) have increased. Issues with reliability and survivability of WEC designs have previously led to setbacks for private developers including closure and delayed or limited testing of devices [1]. Moreover, component or system failure rates directly affect capital costs, operational costs, and power production. Therefore, designing WECs to withstand highly energetic wave conditions without over-engineering them is critical to overcoming industrial and development challenges and enable their implementation.

This is paper no. 1365, submitted to the SMM (Structural mechanics – materials, fatigue, loadings) track of EWTEC 2019. This work was supported by the OES/INORE Blue Energy Collaborative Scholarship

C.E. Clark and B. DuPont are affiliated with the School of Mechanical, Industrial, and Manufacturing Engineering and the Pacific Marine Energy Center at Oregon State University, Corvallis, OR 97331 USA (e-mails: clarkc@oregonstate.edu, bryony.dupont@oregonstate.edu).

A. Garcia-Teruel and D. Forehand are with the School of Engineering and the Institute for Energy Systems at The University of Edinburgh, Edinburgh EH9 3BF, UK (emails: a.garcia-teruel@ed.ac.uk, d.forehand@ed.ac.uk)

Despite the importance of considering WEC reliability in early design phases, it is often considered secondary to power production. Maximizing power production across sea states can increase revenue potential, but also loads and costs. Thus, there is a design trade-off between power production and component reliability that should be considered throughout the WEC design process. Particularly in device geometry design, there is an opportunity to reduce structural and PTO loads [1]. Optimizing WEC shape for reliability and power could decrease downtime and required maintenance costs. Ensuring that WECs perform as they were designed for their intended lifespan, while decreasing levelized costs of energy, is integral to improving their feasibility.

II. Previous Work

While recently reliability information has been increasingly integrated into WEC design, the body of literature that encompasses WEC optimization is extensive. Therefore, this literature review will focus on the most relevant previous research pertaining to reliability-based geometry optimization of WECs, addressing three research foci: 1) WEC hull geometry optimization for cost and power production, 2) reliability-based design optimization of WEC foundations, and 3) WEC hull geometry effects on varying component loads. Through these three bodies of work, we are able to address the focus of this paper, which is relating critical component reliability to WEC hull geometry optimization. For more information on how reliability information is and can be integrated into structural and mechanical design and analysis of WECs, refer to References [2]–[5].

First, WEC hull geometries have been optimized for cost and power production, where costs varied with device size [6]–[8]. Most geometry optimisation studies were based on simple shape definitions such as using cylinders or spheres. A method employing bi-cubic B-spline surfaces has shown to be able to generate very diverse shapes [6]. This approach has been re-implemented and expanded to be applicable to a range of different cases, where, for example, different combinations of modes-of-motion for energy extraction can be taken into account [9]. Due to the nature of optimisation studies, the existence of optimal solutions and the computation time of the objective function are crucial for their success. For this reason,

previous studies focused mostly on maximising power production and accounted for costs in a simplified way, for example through the hull's submerged volume or surface area. However, reliability was not considered. An initial step towards WEC geometry optimisation including reliability considerations was presented in [10], where Kurniawan et al. included the forces on the hinge of an oscillating surge wave energy converter in the objective function of the optimisation process. The main challenge of including reliability considerations in a WEC geometry optimisation process is to find a method that represents the impact of reliability on the WEC design, while doing so in a computationally efficient way.

Second, reliability has been incorporated into WEC design optimization, where the focus has been on both structural and mechanical component reliability. Ambuhl et al. optimized foundation diameter and thickness for the WaveStar device given structural pile failure constraints to maximize profitability [5]. WEC hull shape was not considered, and failure was considered as a constraint of the optimization problem, rather than an objective. In this study, fatigue failures were identified to be a common failure mode in WECs, occurring at welded joints or corroded bolts. Yang et al. focus on a point absorber Power Take-Off (PTO) system much like the current study. Compared to our structural modeling and analysis of the welded joint between the hull and the piston cylinder, Yang et al. use an abrasion model to model the wear of the piston ring by the piston cylinder [11]. Although they only consider one sea state, Yang et al. develop methods to address critical component failure in a power take-off system, which can then be later integrated into optimization studies.

Lastly, a few studies have provided insight into the geometry-dependent structural integrity of WECs. Beirao et al. compared three geometries (a sphere, a horizontal cylinder, and a vertical cylinder with a conical bottom) for a heaving buoy of a point absorber and their effect on component loads. Using Finite Element Methods (FEM), they considered loads on the supporting cables and PTO cylinder rod [12]. They found that, compared to a fully submerged buoy or a buoy floating at the surface, a partially submerged buoy experienced the greatest stresses and excursion. When the piston was retracted the highest loads were observed in the cables, whereas in extended position both rod and cables were identified as critical components. The sphere showed the lowest stress values in both cases. Van Rij et al. [13] compared the resulting PTO DELs from two point absorber floater geometries (a vertical cylinder with truncated conical bottom and a rhombus) and two mooring configurations (a monopile and a spar-plate configuration). Using CFD to obtain viscous drag coefficients for the WECs, Van Rij et al. generated PTO force data from the time-domain model in WEC-Sim. The rhombus float with a spar-plate configuration resulted in the lowest fatigue loads. These two studies inform our understanding of how WEC geometry relates to various component reliability. They, however, employed FEM and CFD models, which are too computationally demanding to be used within an optimization process.

This previous literature has enabled the current work, which addresses the opportunity to implement reliability-based design optimization of hull geometries to design more optimal WECs. This would allow for hull geometries with advantageous reliability scores to be prioritized, balancing cost, power production, and reliability objectives. However, to develop this optimization approach, we first need to develop analysis methods that relate environmental loads the WEC experiences to its reliability, as well as evaluate the sensitivity of its reliability to varying hull geometries. In this study, we will explore the relationship between WEC floater geometry and PTO reliability, focusing on developing an assessment method to evaluate PTO damage at the welded joint between the hull and the piston.

To complete this analysis, we leverage previous work that generates WEC hull geometries and performs hydrodynamic analysis, from which power production and PTO-forces for each geometry can be obtained [6], [9]. From this PTO-force time series, we use Rainflow Counting and appropriate S-N Curves to count the number of fatigue cycles and relate it to Damage Equivalent Load (DEL) metrics. Investigating various WEC hull geometries will allow us to evaluate and compare several hull shapes and their resulting PTO damage. This study will provide insight about how hull geometries affect PTO damage, and enable future work incorporating this reliability assessment method within a geometry optimization process.

This study is divided into three sections. First, the methodology is described in Section III, which 1) defines the case studies, met-ocean conditions, and WEC system characteristics, 2) describes the hydrodynamic model used to determine the PTO-force time series for each case, and 3) details how we calculated the fatigue DELs based on that PTO-force time series. The results for all the cases are presented in Section IV, and the drawn conclusions and planned future work follow in Section V.

III. Methodology

To investigate the effect of WEC hull geometries on PTO DELs, we consider three different floater shapes, two energy absorption modes, and two geographic locations. We introduce the met-ocean conditions and the main characteristics of the WEC-system in Subsection III-A. Subsection III-B details the hydrodynamic model used to generate the PTO force time series. Concluding, Subsection III-C describes our fatigue analysis methods.

A. WEC system definition

In this study, we analyze a point absorber type WEC oscillating in a single mode of motion (either heave, or surge). The WEC floater reacts against a PTO, such as a linear generator or a hydraulic piston, fixed 1) perpendicular to the sea bed, or 2) perpendicular to some vertical surface in the water column (see

Figure 1). We assume the PTO system is composed of a moving rod welded to the floating body and a fixed component. Three different floater shapes were considered: a sphere, a barge, and a cylinder. We chose the dimensions of the three shapes so that their draft and characteristic width would be equivalent. These dimensions are also shown in Figure 1.

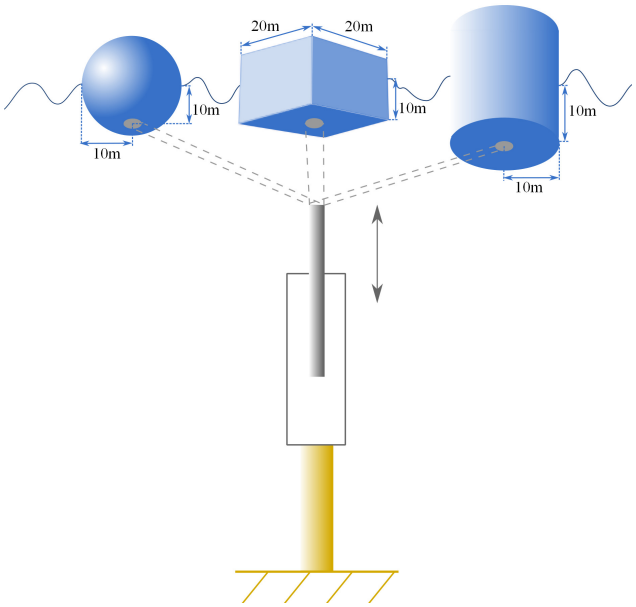

(a) Heave

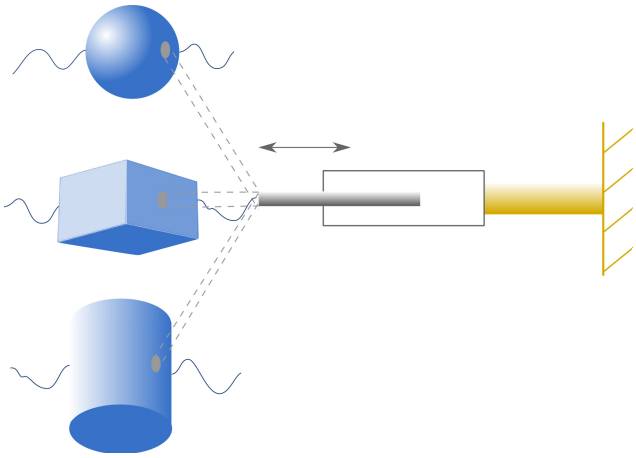

(b) Surge

Fig. 1. Schematic representation of the WEC systems oscillating in (a) heave and (b) surge.

B. Hydrodynamic Modelling

To model the sea states of the two locations, we first derived the characteristic sea states at each location, and then used the resulting significant wave height H_s, peak period T_p, and probability of occurrence as input for the WEC hydrodynamic model.

1) Study Areas and Sea State Conditions: To model the hydrodynamics of this system, we considered two geographic locations, each with their own set of characteristic sea states. We considered sea states 1) in the central North Sea and 2) off the southwestern coast of Norway (Figure 2). These two locations correspond to Site 15 and Site 14, respectively, of the European Union's MARINA Project (or Marine Renewable Integrated Application Platform) [14]. They were chosen for the availability of metocean data, as well as because their site conditions are distinct enough to compare WEC response dependence on location. For instance, the sites differ significantly in the average depth at the site, the level of protection from open ocean conditions, and the shape of the sea state conditions distribution. These site conditions are described in Table I.

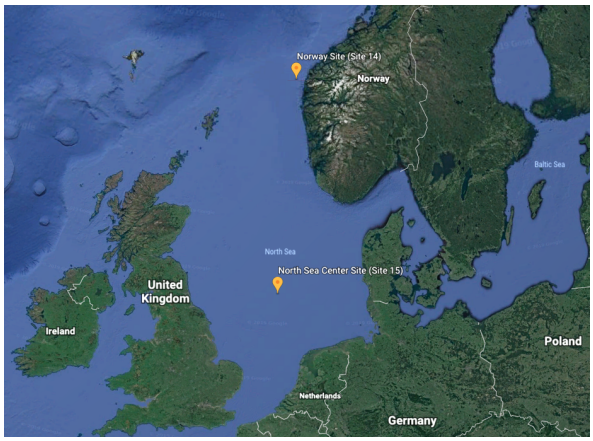

Fig. 2. Site Locations: North Sea Center and Norway.

TABLE I
SITE CHARACTERISTICS

	North Sea	**Norway**
Location	55.13N, 3.43E	61.85N, 4.23E
Water Depth (m)	29	200
Distance to shore (km)	300	30
50-year U_w at 10 m (m/s)	27.2	33.49
50-year H_s (m)	8.66	10.96
Mean value of T_p (s)	6.93	11.06

The MARINA Project provides marginal and joint distributions of wind and wave data for the study locations. The National and Kapodistrian University of Athens provided the 10 years (2001-2010) hourly raw data for the selected offshore sites. Both marginal and joint distributions are obtained by fitting analytic solutions to raw data and are characterized by one-hour mean wind speed at 10 m above mean sea level (U_w), significant wave height (H_s) and spectral peak period (T_p) [15].

The joint Probability Density Function (PDF) of U_w, H_s, and T_p is defined by the marginal PDF of U_w (fU_w), a PDF of H_s conditional on U_w ($fH_s|U_w$) and a PDF of T_p conditional on H_s ($fT_p|H_s$). The parameters and equations that define these distributions can be found in the original description of the site conditions [15]. The resulting representative sea states are described in Table II and III. For the purposes of this study, we assume the waves are unidirectional, approaching the WEC from the west.

2) PTO Force estimation: To estimate the PTO-force, the WEC motion at each location was analysed with a frequency-domain model. The model is based on linear wave theory, where wave height is assumed to be

TABLE II
SEA STATE CONDITIONS FOR THE NORTH SEA SITE

	$\mathbf{H}_s$ [m]	$\mathbf{T}_p$ [s]	Probability [%]	Occurrence [h/year]
1	0.64	6.06	13.1	1145
2	0.73	6.13	8	698.2
3	0.77	6.17	2.1	186.2
4	0.8	6.19	0.3	27.9
5	1.26	6.55	5.8	512
6	1.43	6.68	17.3	1517.4
7	1.56	6.78	13.2	1154.3
8	1.63	6.83	3.9	344.4
9	1.66	6.86	0.6	55.9
10	1.69	6.88	0.1	9.3
11	2.22	7.28	1.9	167.6
12	2.37	7.4	9.5	828.5
13	2.51	7.5	8.5	744.7
14	2.58	7.56	2.6	223.4
15	2.61	7.58	0.3	27.9
16	3.21	8.05	0.6	55.9
17	3.35	8.16	3.9	344.4
18	3.48	8.26	3.5	307.2
19	3.55	8.32	1	83.8
20	3.59	8.35	0.1	9.3
21	4.21	8.85	0.2	18.6
22	4.35	8.96	1.4	121.09
23	4.47	9.06	1.1	93.1
24	4.54	9.11	0.2	18.6
25	5.22	9.68	0.1	9.3
26	5.36	9.8	0.4	37.2
27	5.47	9.89	0.2	18.6

TABLE III
SEA STATE CONDITIONS FOR THE NORWAY SITE

	$\mathbf{H}_s$ [m]	$\mathbf{T}_p$ [s]	Probability [%]	Occurrence [h/year]
1	0.67	9.48	3.3	282.2
2	0.7	9.51	3.9	335
3	0.73	9.55	1.1	92.7
4	0.77	9.59	0.1	9.5
5	1.5	10.3	7.2	615.9
6	1.54	10.33	12.5	1070.4
7	1.58	10.36	5.6	479.2
8	1.62	10.39	0.9	79.2
9	1.65	10.41	0.1	5.4
10	2.42	10.94	4.4	374.7
11	2.46	10.96	12.1	1035.5
12	2.51	10.99	9.4	806.9
13	2.56	11.02	2.5	212.9
14	2.59	11.04	0.2	21.3
15	3.35	11.46	1.1	93.7
16	3.4	11.48	5.3	541.4
17	3.46	11.51	8.2	699.5
18	3.52	11.54	3.8	327.5
19	3.56	11.56	0.6	49.4
20	4.3	11.91	0.1	10.1
21	4.34	11.93	1.1	92.2
22	4.41	11.96	3.8	326.4
23	4.48	11.99	3.7	315.4
24	4.53	12.01	0.9	479.8
25	4.56	12.03	0.1	6.4
26	5.29	12.33	0.1	8.6
27	5.36	12.36	0.9	78.9
28	5.43	12.39	2.2	185.5
29	5.5	12.42	1.1	91.7
30	5.54	12.44	0.1	11.3
31	6.3	12.73	0.1	9.3
32	6.38	12.76	0.7	62.4
33	6.46	12.79	0.8	72
34	6.52	12.81	0.2	15.6
35	7.33	13.11	0.1	11
36	7.42	13.14	0.4	36
37	7.49	13.16	0.2	16.3
38	8.37	13.46	0.1	10.4
39	8.46	13.49	0.1	12.1
40	9.42	13.81	0.1	5.9

much smaller than wave length and water depth, and oscillations are assumed to be small. In this case, waves are represented as harmonic oscillations of different wave height and frequency, which can be linearly superposed to represent an irregular sea. For each sea state the relation of wave amplitude to frequency is defined by a Bretschneider spectrum, where 150 frequencies (ω_k) from 0 to 3 rad/s in 0.02 steps are analysed.

It should be noted that non-linear effects are not considered when using this method. This could lead to both under- or overestimation of the experienced forces. However, in [16], it was found that linear theory tends to overestimate the WEC dynamic response and absorbed power. With the purpose of developing a method suitable for hull geometry optimization at early design stages, the considered assumptions seem reasonable to provide upper limits of the system performance, while taking into account PTO-reliability.

Under these assumptions, the equation of motion of a WEC can be written as in (1), where the main forces affecting the motion will be the wave excitation force $\mathbf{F}_e$, the PTO-force $\mathbf{F}_{PTO}$, the WEC inertia $\mathbf{M}$, the radiation force composed of an added mass $\mathbf{M}_{rad}$ and an added damping $\mathbf{C}_{rad}$ terms, and the hydrostatic force represented by a stiffness term $\mathbf{K}_H$ following Archimedes principle. An additional damping term $\mathbf{C}_{loss}$ is included to represent friction losses as in [6]. The stiffness value from the mooring lines is neglected, because it is considered to be much smaller than the hydrostatic stiffness value.

$$\begin{aligned}\hat{\mathbf{F}}_e + \hat{\mathbf{F}}_{PTO} =&[-\omega^2(\mathbf{M}+\mathbf{M}_{rad}) + i\omega(\mathbf{C}_{rad}+\mathbf{C}_{loss}) \\ &+ \mathbf{K}_H]\hat{\mathbf{X}}(\omega_k)\end{aligned} \tag{1}$$

An idealised optimal control strategy is assumed, which sets the mass, damping and stiffness terms composing the PTO-force to match the impedance $\mathbf{Z}$, as defined in (2), at the energy period $T_e = 2\pi/\omega_e$. Here $\hat{\mathbf{U}}$ represents a vector of complex amplitudes of the oscillation velocity in six degrees of freedom, and $\hat{\mathbf{X}}$ is the corresponding vector of complex amplitudes of oscillation.

$$\hat{\mathbf{F}}_e = \mathbf{Z}\hat{\mathbf{U}} = \mathbf{Z}i\omega\hat{\mathbf{X}} \tag{2}$$

Then the PTO-force is defined by the complex conjugate of the impedance $\mathbf{Z}^*$ as shown in (3).

$$\begin{aligned}\hat{\mathbf{F}}_{PTO} &= -\mathbf{Z}^*\hat{U} = -\mathbf{Z}^* i\omega\hat{\mathbf{X}} \\ &= [-\omega^2(\mathbf{M}+\mathbf{M}_{rad}(\omega_e)) - i\omega(\mathbf{C}_{rad}(\omega_e)+\mathbf{C}_{loss}) \\ &\quad + \mathbf{K}_H]\hat{\mathbf{X}}\end{aligned} \tag{3}$$

The time series of the PTO-force $F_{PTO_{s,q}}(t)$ can then be obtained for each sea state s and set q of random phase shifts $\psi_{s,k,q}$ from the superposition of the single harmonic force representations at each frequency ω_k.

$$\begin{aligned}F_{PTO_{s,q}}(t) = \sum_{k=1}^{N} \Big(&\Big|\hat{F}_{PTO_s}(\omega_k)\Big| \cos(\omega_k t + \psi_{s,k,q} \\ &+ \angle\hat{F}_{PTO_s}(\omega_k)\Big)\end{aligned} \tag{4}$$

Here $\hat{F}_{PTO_{\hat{s}}}$ represents each sea state component s of the vector $\hat{\mathbf{F}}_{PTO}$.

PTO-stroke constraints were first considered by setting the PTO-force to zero when the maximum stroke (5m) was exceeded, since it was assumed that the end stops would be taking all the load in this situation. It was found that setting the force to zero when the stroke limit is reached, might favour highly oscillating shapes. In those cases the DEL will not be representative for PTO reliability, because the end stops are not designed to be hit every 10 seconds. Within an optimization process the aim is to generate shapes, with a good trade-off between large enough oscillations for power production but small enough to minimize DEL. It is, therefore, recommended to not include this type of constraint for a better representation of the PTO reliability. PTO-stroke and rating constraints are, however, assumed here to calculate the average annual power as in [9], but are considered to have no effect on the PTO-force time series.

An example of the PTO-force time series for a heaving cylinder in the North Sea can be seen in Figure 3, where sea states are numbered according to Table II.

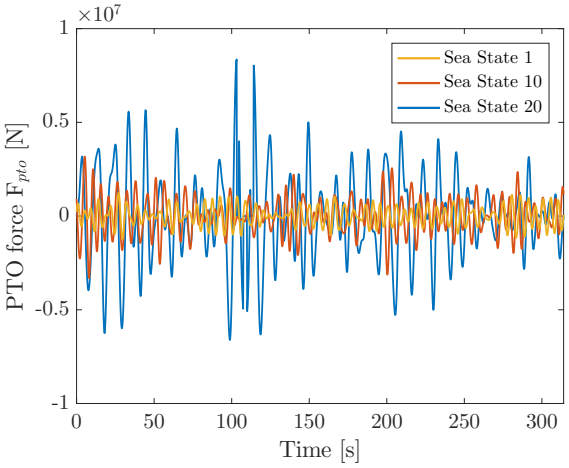

Fig. 3. PTO force time series for a heaving cylinder in the North Sea for three different sea states.

C. Fatigue Damage Analysis

In total, 10 PTO-force time series were generated for each case and wave condition, resulting in 1620 time series for the North Sea cases and 2400 time series for the Norway cases. Descriptions of these 12 cases are in Table VI.

For our analysis, we focused on the fatigue failure of the rod weld connecting the floater to the PTO. Fatigue failures are speculated to be a common failure mode in WECs, occurring at welded joints or corroded bolts [5]. Furthermore, this type of failure has high technical and economic consequence, with the failure of the weld causing complete failure of the device and costly repair via re-welding either at sea or in port.

After generating the force time series for a given case and sea state, we used the area of the PTO piston rod connecting to the hull to convert the force into stress. With the stress time series, we counted the number of stress cycles in that series with WAFO's [17] Rainflow Counting algorithm. We then used S-N curves to determine the cycles to failure of the weld given our selected material, the type of weld, and the magnitude of the stress cycles. We use DNV Standards on Fatigue Design of Offshore Steel Structures [18], specifically S-N Curve D in Table A5 for stress perpendicular to the weld, with a traverse splice in rolled sections. This curve assumes the weld is subject to seawater and has cathodic protection.

TABLE IV
DEFINITION OF CASES

Case	Location	Motion	Shape
1	North Sea	Heave	Cylinder
2	North Sea	Heave	Sphere
3	North Sea	Heave	Barge
4	North Sea	Surge	Cylinder
5	North Sea	Surge	Sphere
6	North Sea	Surge	Barge
7	Norway	Heave	Cylinder
8	Norway	Heave	Sphere
9	Norway	Heave	Barge
10	Norway	Surge	Cylinder
11	Norway	Surge	Sphere
12	Norway	Surge	Barge

We binned the counted stress cycles by their amplitudes in 20 bins, as suggested by Wægter [19]. We then used Palmgren-Miner's rule to estimate the accumulated damage, or weld fatigue caused by each binned stress range for each sea state. That is, for each bin, we divide the number of cycles in that bin by the number of cycles to failure for the given stress range. The cycles to failure, or the component capacity against fatigue, is determined by Eq. 5.

$$n_c(s) = a_D s^{-m} \tag{5}$$

where $n_c(s)$ is the number of stress ranges (or the number of cycles) in a given amplitude, a_D is the intercept parameter of the S-N curve, s is the stress range (double the amplitude) in MPa, and m is the slope of the S-N Curve. These S-N Curve and Rainflow Counting details are included in Table V.

TABLE V
FATIGUE ANALYSIS DETAILS

Parameter	Value
a_D	11.764e6
m	3
Rod Diameter (m)	6
Number of Force Range Bins	20
Lifespan (years)	20

The results for each sea state are then multiplied by the expected number of times they occur during the lifetime of the structure to obtain a measure of the total fatigue damage. We repeat this for each case with 10 PTO-force time series to gain an understanding of the variation in fatigue DEL, due to the random superposition of the wave frequency components.

IV. RESULTS & DISCUSSION

In this section, we separate our results by whether the WEC is heaving or surging and by its location

(North Sea and Norway). The results are presented in terms of DEL absolute numbers, as well as normalised by the shapes' respective submerged volumes. This is done to eliminate the effect that the difference in submerged volume might have on fatigue results.

A. North Sea site

Figure 4 represents DEL results for the two motions of oscillation in the North Sea. Across the site-specific sea states, the heave case has lower DELs than surge case.

In both cases the trend of the Response Amplitude Operator (RAO) in heave and surge is reflected in the trends of the DELs. The DEL in heave increased with sea state. Figure 5 (a) indicates that the oscillation also increased with sea state. In the surge case a peak in DEL can be seen at sea state 22. This coincides with the resonance period shown in Figure 5 (b). In conclusion, a relation between DEL behaviour, and RAO depending on period can be observed, that sets the overall pattern of the DEL.

When considering the DELs across shapes, the sphere results in higher DELs in the heaving case at high sea states, but the cylinder and barge have higher DELs at lower sea states. In the surging case, the cylinder and barge have consistently higher DELs than the sphere. However, the sphere shows the highest submerged volume normalised DELs in both, heave and surge, followed by the cylinder and then the barge. This is the case, because the sphere has the lowest submerged volume, followed by the cylinder and then the barge, which has two times the sphere's submerged volume.

B. Norway site

Figure 6 depicts the DELs for the two motions of oscillation at the Norway site. Here, contrary to the North Sea, higher DELs are obtained in the heave case than in the surge case.

Here again the trend of the RAO is reflected in the shape of the DEL diagrams. In the heaving case, an increase in DEL with sea state can be observed, which matches with the increasing RAO with period shown in Figure 7 (a). In surge, a peak in DEL can be observed in sea state 15, which coincides with resonance period shown in Figure 7 (b). The DEL is otherwise highest at middle-range sea states (20 to 24), which are slightly more energetic than sea state 15. There, T_p is between 11.9 and 12s, which still corresponds to the range of higher RAO's in Figure 7 (b).

When considering the DELs across shapes, in both heave and surge, the highest DELs are consistently achieved by the barge, followed by the cylinder and then the sphere. However, when looking at the submerged volume normalised DELs, in heave the order inverts with the sphere showing consistently the highest values.

C. Across sites

The highest DELs are achieved in the heaving case in Norway, at the most energetic sea state. In the surging case the highest value is achieved in the North Sea in sea state 22. It can be observed that peaks in DEL coincide either with higher energetic sea states (Norway, heave, sea state 40) or with higher probability of occurrence of relatively high energetic sea states (North sea, surge, sea state 22).

In the North Sea, the peak period T_p ranges from 6.06 to 9.89, whereas in Norway sea states start at a higher peak periods with a range from 9.48 to 13.81s. When comparing, for instance, the heave RAOs of the three shapes, it can be observed that in Norway the RAO values are two times the ones in the North Sea for the relevant period range, which is reflected also in the difference in DELs for these two cases. This trend can also be observed in surge to a lower extent.

In the surging cases it can be observed that all shapes show a very similar performance when the DELs are normalised to the submerged volume. In the heaving case this is rather the opposite. The differences in DEL results become more accentuated when normalised to the submerged volume. This could point to a stronger dependency of DEL results from submerged volume in the surging case, and from shape in the heaving case.

Overall the performance of the different shapes, can be analysed considering also their annual average power production, shown in Table VI. The results indicate that the barge shape has the highest DELs across most cases and sea states, although it also achieves the highest power production in Norway in both heave and surge, and the second highest in the North Sea, when compared to the other shapes. The reason for this, can be the higher submerged volume of the barge, which is approximately two times the submerged volume of the sphere and 1.2 times the submerged volume of the cylinder. In contrast, the spherical shape has the lowest DELs across most cases and sea states (agreeing with Beirao's results [12]), and produces the highest power in the North Sea in both heave and surge, and performs similarly to the barge in Norway. However, when looking at the submerged volume normalised DELs the sphere has the highest DELs in the North Sea and in the heaving case in Norway. This shows that the sphere with a lower volume than the barge achieves better overall results. When taking into account its submerged volume the sphere performs worse in terms of DELs, but better in terms of power.

TABLE VI
POWER PRODUCTION ACROSS CASES

Case	Location	Motion	Shape	Average Power [kW]
1	North Sea	Heave	Cylinder	143
2	North Sea	Heave	Sphere	158
3	North Sea	Heave	Barge	145
4	North Sea	Surge	Cylinder	29
5	North Sea	Surge	Sphere	35
6	North Sea	Surge	Barge	30
7	Norway	Heave	Cylinder	547
8	Norway	Heave	Sphere	591
9	Norway	Heave	Barge	592
10	Norway	Surge	Cylinder	428
11	Norway	Surge	Sphere	524
12	Norway	Surge	Barge	528

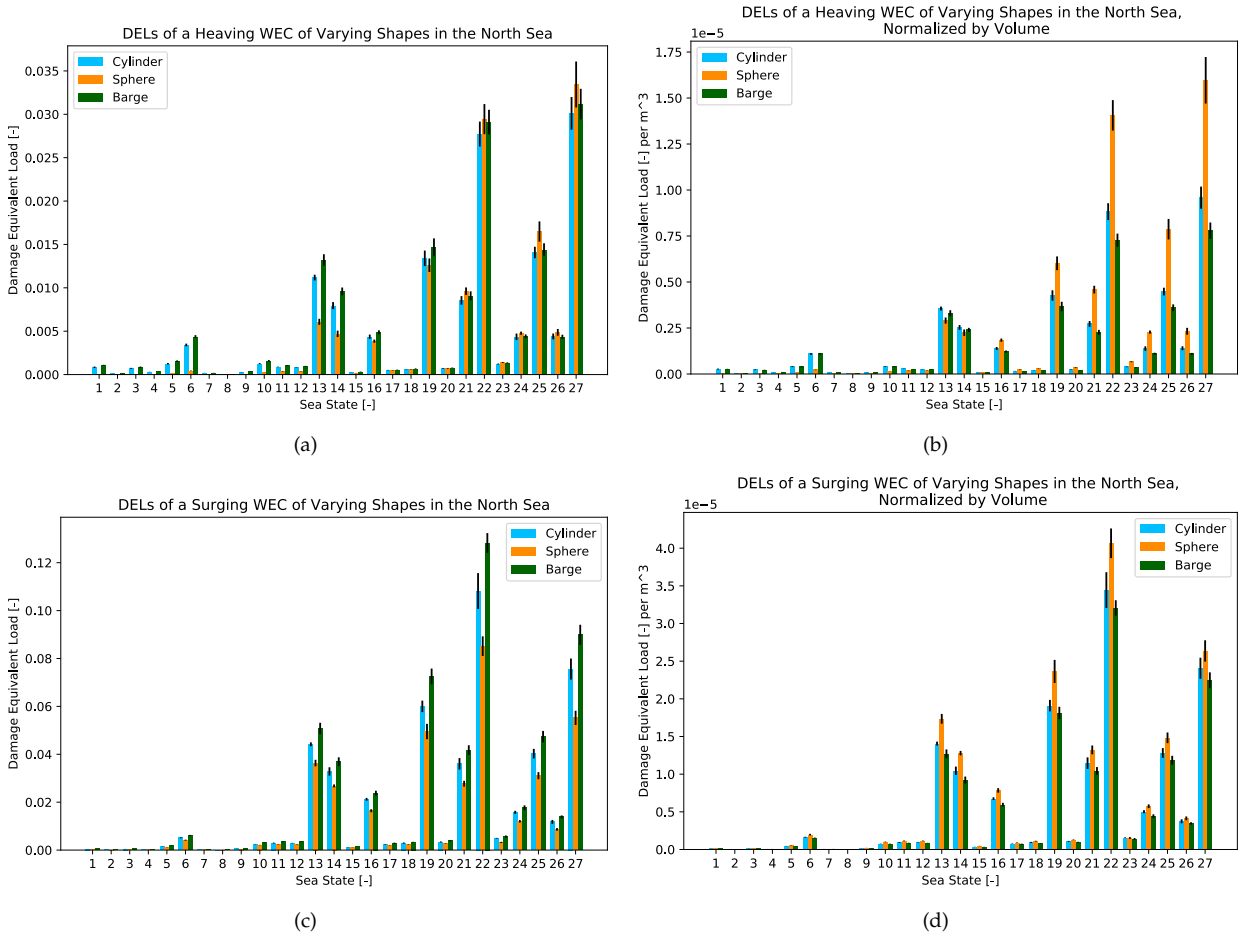

Fig. 4. Damage equivalent loads across sea states for a WEC of varying shapes in the North Sea oscillating in (a) heave and (b) normalized by volume, as well as in (c) surge and (d) normalized by volume.

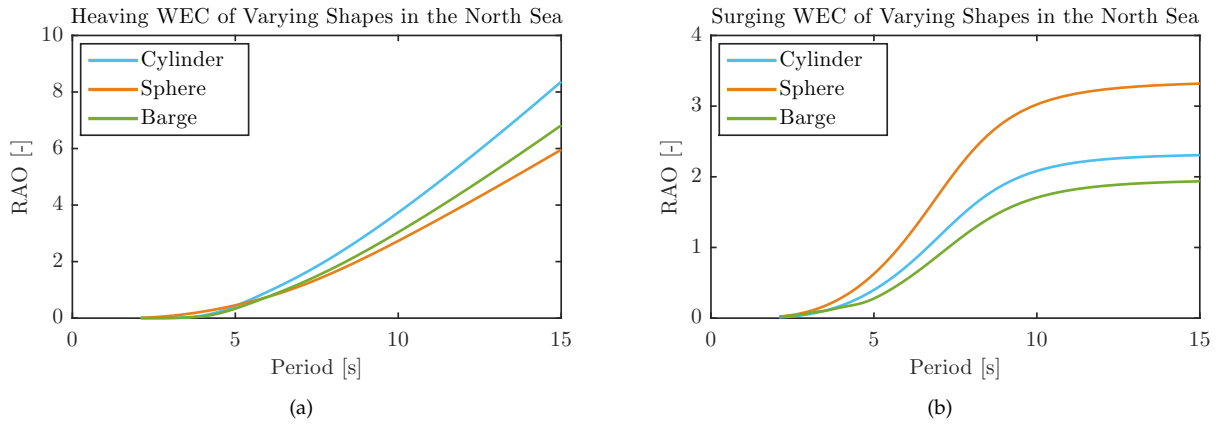

Fig. 5. RAOs of the different hull shapes in the North Sea oscillating in (a) heave and (b) surge.

V. Conclusions

In this study, we explore the relationship between WEC floater hull geometry and PTO reliability. We analyse 12 cases in total, across two locations (North Sea and Norway), two modes of motion (heave and surge), and three shapes (barge, cylinder, and sphere). Based on these conditions, we measure the damage equivalent load (DEL) on the rod weld connecting the floater to the PTO.

Results indicate a clear dependence of DELs on location, oscillation direction, and shape. Therefore, it is critical to consider these parameters in the early design of WECs. Moreover, this study makes the case for incorporating reliability objectives into early design simultaneously with power production and cost, rather than secondary to them. Incorporating reliability in conjunction with power production and cost objectives will enable developers and researchers to design more optimal WECs, advancing the techno-economic feasibility of this technology.

Within a WEC hull geometry optimization process, the aim is to generate shapes that result in the optimal

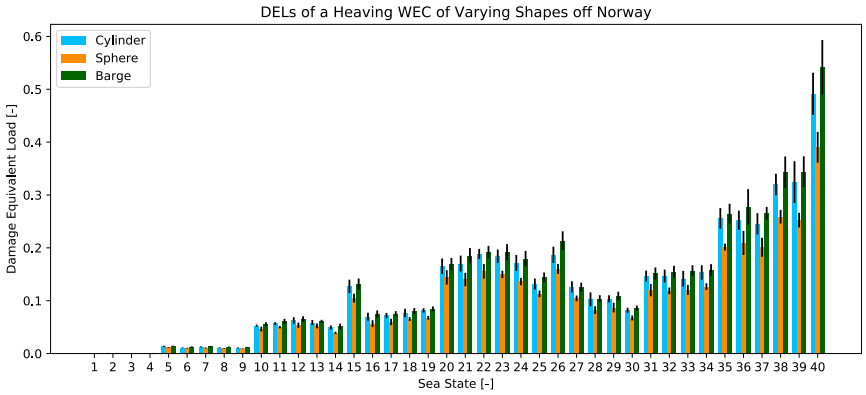

(a)

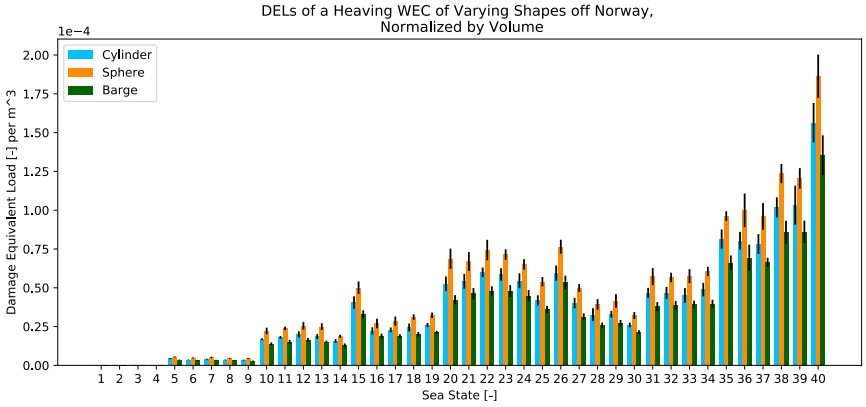

(b)

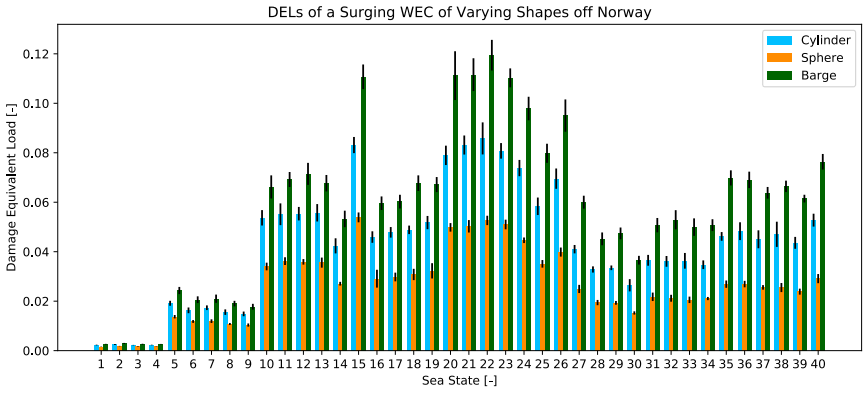

(c)

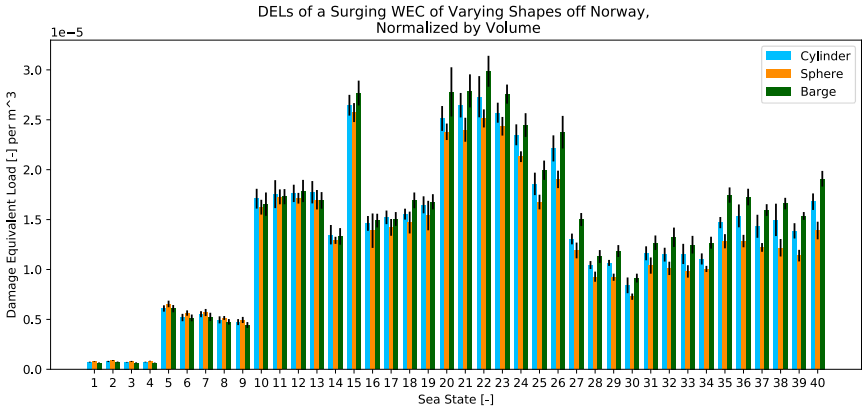

(d)

Fig. 6. Damage equivalent loads across sea states for a WEC of varying shapes off Norway oscillating in (a) heave and (b) normalized for volume, as well as in (c) surge and (d) normalized for volume.

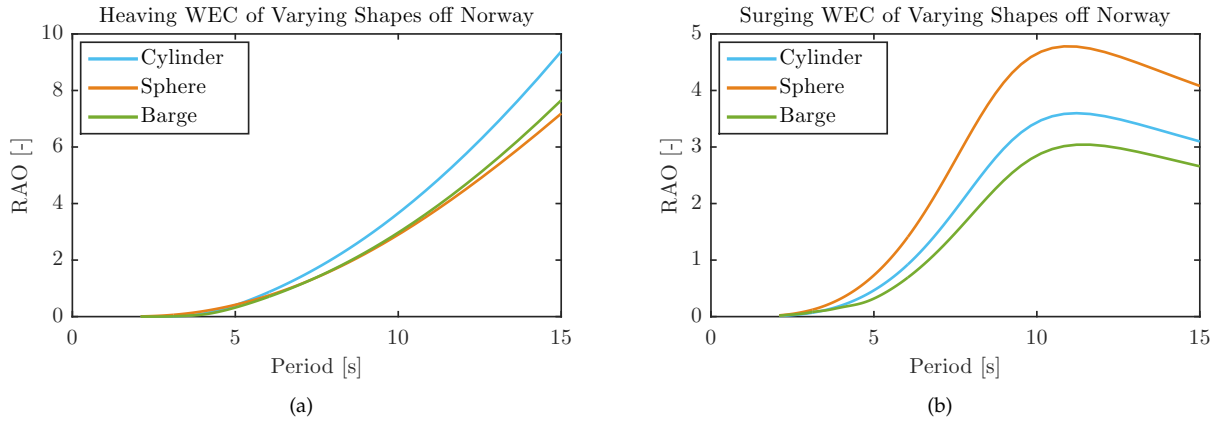

Fig. 7. RAOs of the different hull shapes off Norway oscillating in (a) heave and (b) surge.

balance of large enough oscillations for power production while minimising fatigue effects on the hull-PTO connection. For this reason, as found during this study, the inclusion of PTO-stroke constraints in the calculation of the force time series when using this method is not recommended, since it could lead to miss-leading results.

In future work, we plan to expand upon the methods included in this study to use a more detailed PTO model. More importantly, this study will be used as the basis for future reliability-based design optimization work that optimizes WEC floater hull geometry to improve PTO reliability, power production, and cost.

REFERENCES

[1] R. Coe, Y.-H. Yu, J. van Rij, R. G. Coe, Y.-H. Yu, and J. van Rij, "A Survey of WEC Reliability, Survival and Design Practices," *Energies*, vol. 11, no. 1, p. 4, dec 2017. [Online]. Available: http://www.mdpi.com/1996-1073/11/1/4

[2] C. E. Clark and B. DuPont, "Reliability-based design optimization in offshore renewable energy systems," *Renew. Sustain. Energy Rev.*, vol. 97, no. June, pp. 390–400, 2018. [Online]. Available: https://doi.org/10.1016/j.rser.2018.08.030

[3] J. Wolfram, "On Assessing the Reliability and Availability of Marine Energy Converters: The Problems of a New Technology," *Risk Reliab.*, vol. 220, 2006.

[4] P. R. Thies, *Reliability of wave energy converters*, 2009.

[5] S. Ambühl, M. Kramer, and J. D. Sørensen, "Reliability-Based Structural Optimization of Wave Energy Converters," *Energies*, vol. 7, pp. 8178–8200, 2014. [Online]. Available: www.mdpi.com/journal/energies

[6] A. McCabe, "Constrained optimization of the shape of a wave energy collector by genetic algorithm," *Renew. Energy*, vol. 51, pp. 274–284, mar 2013. [Online]. Available: http://www.sciencedirect.com/science/article/pii/S0960148112006258

[7] M. Blanco, P. Moreno-Torres, M. Lafoz, and D. Ramírez, "Design parameter analysis of point absorber WEC via an evolutionary-algorithm-based dimensioning tool," *Energies*, vol. 8, no. 10, pp. 11 203–11 233, 2015.

[8] A. Babarit and A. H. Clément, "Shape optimisation of the SEAREV wave energy converter," *9th World Renew. Energy Congr.*, 2006.

[9] A. Garcia-Teruel and D. Forehand, "Optimal wave energy converter geometry for different modes of motion," in *Adv. Renew. Energies Offshore Proc. 3rd Int. Conf. Renew. Energies Offshore (RENEW 2018)*, Lisbon, 2018, pp. 299–305.

[10] A. Kurniawan and T. Moan, "Optimal geometries for wave absorbers oscillating about a fixed axis," *IEEE Journal of Oceanic Engineering*, vol. 38, no. 1, pp. 117–130, 2013.

[11] L. Yang, T. Hals, and T. Moan, "A wear model for assessing the reliability of wave energy converter in heave with hydraulic power take-off," *Proc. 8th Eur. Wave Tidal Energy Conf.*, no. September, pp. 874–881, 2009.

[12] P. J. B. F. N. Beirão and C. M. dos Santos Pereira Malça, "Design and analysis of buoy geometries for a wave energy converter," *Int. J. Energy Environ. Eng.*, vol. 5, no. 2-3, p. 91, jul 2014. [Online]. Available: http://link.springer.com/10.1007/s40095-014-0091-7

[13] J. van Rij, Y.-H. Yu, K. Edwards, and M. Mekhiche, "Ocean power technology design optimization," *Int. J. Mar. Energy*, vol. 20, pp. 97–108, dec 2017. [Online]. Available: https://www.sciencedirect.com/science/article/pii/S2214166917300656

[14] M. Sojo Armentia and G. Auer, "MARINA Platform Final Summary Report," Tech. Rep., 2014.

[15] L. Li, Z. Gao, and T. Moan, "Joint Environmental Data at Five European Offshore Sites for Design of Combined Wind and Wave Energy Devices," *Vol. 8 Ocean Renew. Energy*, vol. 8, no. 7491, p. V008T09A006, 2013. [Online]. Available: http://www.scopus.com/inward/record.url?eid=2-s2.0-84893074848{\&}partnerID=tZOtx3y1

[16] A. Babarit, J. Hals, M. Muliawan, A. Kurniawan, T. Moan, and J. Krokstad, "Numerical benchmarking study of a selection of wave energy converters," *Renew. Energy*, vol. 41, pp. 44–63,

may 2012. [Online]. Available: http://www.sciencedirect.com/science/article/pii/S0960148111005672

[17] The WAFO Group, "WAFO—a Matlab toolbox for analysis of random waves and loads," Lund University, Lund, Sweden, Tech. Rep. March, 2011. [Online]. Available: http://www.maths.lth.se/matstat/wafo/documentation/wafoiso.ps

[18] DNV, "RP-C203- Fatigue design of offshore steel structures," *Recomm. Pract. DNV-RPC203*, no. October, p. 126, 2014. [Online]. Available: ftp://128.84.241.91/tmp/MSE-4020/Fatigue-Design-Offshore.pdf

[19] J. Waegter, "Stress range histories and Rain Flow counting," 2009, no. June, pp. 1–13.